Interdisciplinary Research in Medical Sciences Specialty
ISSN: 3062-4401
2026, Volume 6, Issue 1, Page No: 207-223

Available online at: www.galaxypub.co/page/journals

Galaxy Publication

Sympathetic–Parasympathetic Nerve Interplay in Gastric Cancer Development

Nora Schneider[1]*, Tobias Frank[1], Andreas Müller[2], Christoph Meier[3]

[1]Department of Neuro-Oncology and Gastric Cancer, Faculty of Medicine, University of Freiburg, Freiburg, Germany.
[2]Department of Autonomic Nervous System and Tumorigenesis, Faculty of Medicine, Heidelberg University, Heidelberg, Germany.
[3]Department of Nerve–Tumor Interactions, Faculty of Medicine, University of Hohenheim, Stuttgart, Germany.

***E-mail** ✉ nora.schneider@natfak.uni-freiburg.de

Received: 23 February 2026; **Revised:** 10 May 2026; **Accepted:** 15 May 2026

ABSTRACT

Latest findings stress how vital the nervous system is for tumors to advance. Still, knowledge about the specific ways nerves affect the start and growth of stomach cancers stays quite incomplete. This project intends to uncover shifts in nerve presence, the main genes connected to them, and the key signaling routes active while gastric tumors form. We included 257 people who had gastric precancerous lesions (GPLs) drawn from four separate national patient groups. Using immunohistochemistry staining plus computer-assisted measurement, we determined the amounts of sympathetic nerves, parasympathetic nerves, and Schwann cells present in the collected tissue sections. We also pulled three sets of mRNA expression data for GPL tissues from the Gene Expression Omnibus database. These were examined for nerve-linked gene activity patterns, genes showing changed expression levels, enriched biological routes, and features of the surrounding immune environment. Parasympathetic nerve density and Schwann cell numbers rose steadily, but sympathetic nerve density moved in the reverse direction as the precancerous stages advanced. In particular, the combined suppression of CD8+ T cells, natural killer cells, and antigen-presenting cells (APC) lessened, while epithelial-mesenchymal transition climbed sharply when moving from initial to later premalignant phases. A group of central genes controlling nerves (NTRK3, MYBL2, NRP1, BCL2, CCND1, VEGFA, PLXNA2, ADRB2) together with certain pathways (mitogen-activated protein kinase [MAPK]/ERK, PI3K/AKT, Wnt) stood out as probable drivers of precancerous development. The work shows an evolving balance between sympathetic and parasympathetic nerves, with parasympathetic nerves and Schwann cells becoming gradually denser while sympathetic nerves follow an opposing downward course through the precancerous stages. Interfering with the mutual effects between cancer cells and nerves—especially the sympathetic and parasympathetic varieties—has surfaced as an encouraging tactic for stopping and treating gastric cancer.

Keywords: Bioinformatics, Gastric precancerous lesion, Immunohistochemistry, Parasympathetic nerve, Schwann cell, Sympathetic nerve

How to Cite This Article: Schneider N, Frank T, Müller A, Meier C. Sympathetic–Parasympathetic Nerve Interplay in Gastric Cancer Development. Interdiscip Res Med Sci Spec. 2026;6(1):207-23. https://doi.org/10.51847/hGeCzN5GdF

Introduction

Much like other solid cancers, stomach cancer formation in humans is a complicated, multi-step event guided by the tumor microenvironment (TME) [1, 2]. This microenvironment forms a highly interconnected setting that includes cancer cells, various immune cells, fibroblasts, and cells lining blood vessels. The ongoing exchanges between these parts heavily influence how tumors begin, enlarge, invade nearby areas, spread to distant sites, and react to therapies [3, 4]. Researchers have studied immune cells, blood vessel cells, and surface-lining cells in depth, producing major improvements in precision treatments [5]. Yet the nervous system has only recently drawn attention as a major controller of cancer growth. The mutual signaling between nerves and tumors, known as nerve-cancer crosstalk, is now a growing focus within cancer neuroscience.

Nerves help steer tumor expansion and distant spread inside the TME by sending out neurotransmitters that bind to receptors located on cancer cells and nearby support cells [6]. Cancer cells themselves can reshape nerve behavior and take advantage of nerves to boost their progress [6, 7]. This kind of nerve-tumor interaction has undergone detailed examination in cancers affecting the brain, prostate, head and neck region, and pancreas [8-12]. However, studies addressing the nervous system's part in cancers of the digestive tract have only started appearing more recently [13]. Although invasion along nerves is accepted as an important warning sign for poorer outcomes in several cancers, including gastric cancer (GC) [14-16], scientists still know little about how different nerve categories are arranged and how dense they become as gastric tumors evolve.

For this project we mapped the placement and concentration of nerves at every point along the gastric cancer development sequence. This involved immunohistochemical (IHC) labeling of gastric precancerous lesions (GPLs), healthy stomach tissue, and malignant samples taken through endoscope-guided biopsies or operations from four independent hospital groups. We additionally used gene expression omnibus (GEO) collections to confirm the observed nerve patterns and to search for important genes plus biological routes that manage nerve activity. Our data revealed a changing relationship between sympathetic and parasympathetic nerve supplies as stomach tumors develop. These patterns held up when checked against nerve-related expression signals from mRNA sequencing. Bioinformatics tools also singled out the main nerve-influencing genes and the functional routes they use.

Unlike earlier publications, the present study supplies the first thorough picture of how various nerve signals shift during gastric cancer (GC) formation, relying on samples gathered from multiple medical centers. Special emphasis falls on how sympathetic and parasympathetic nerve densities and Schwann cell populations change across the different precancerous stages. Although past work has recognized nerves' involvement in GC, our effort delivers a more complete look at precise neural adjustments inside the stomach's local environment by merging real-patient group data with mRNA profiles. We also point out new candidate genes and signaling cascades that appear to steer nerve-tumor communication, which could become useful points for future treatments. Clarifying the separate influences of sympathetic versus parasympathetic nerves on precancerous stomach changes gives important clues for creating therapies meant to break nerve-supported tumor growth in GC.

Materials and Methods

Patients, samples and study design

Figure 1 presents an outline of the complete research plan. In total we enrolled 257 suitable patients from four large hospitals located across the country: Nanfang Hospital affiliated with Southern Medical University (Nanfang cohort), the First Affiliated Hospital of Shantou University Medical College (Shantou cohort), Shantou Longhu People's Hospital (Longhu cohort), and Wuhan Central Hospital (Wuhan cohort). Samples came from patients who had endoscopic biopsies or surgery for several kinds of GPLs, such as atrophic gastritis (AG), intestinal metaplasia (IM), low-grade intraepithelial neoplasia (LIN), and high-grade intraepithelial neoplasia (HIN). We additionally collected normal stomach tissue and tumor tissue from individuals with intestinal-type GC. Three GEO datasets (GSE55696, GSE87666, and GSE160116) containing RNA-seq information on human GPLs were downloaded for deeper study. More information on these datasets appears in the Supplementary Methods.

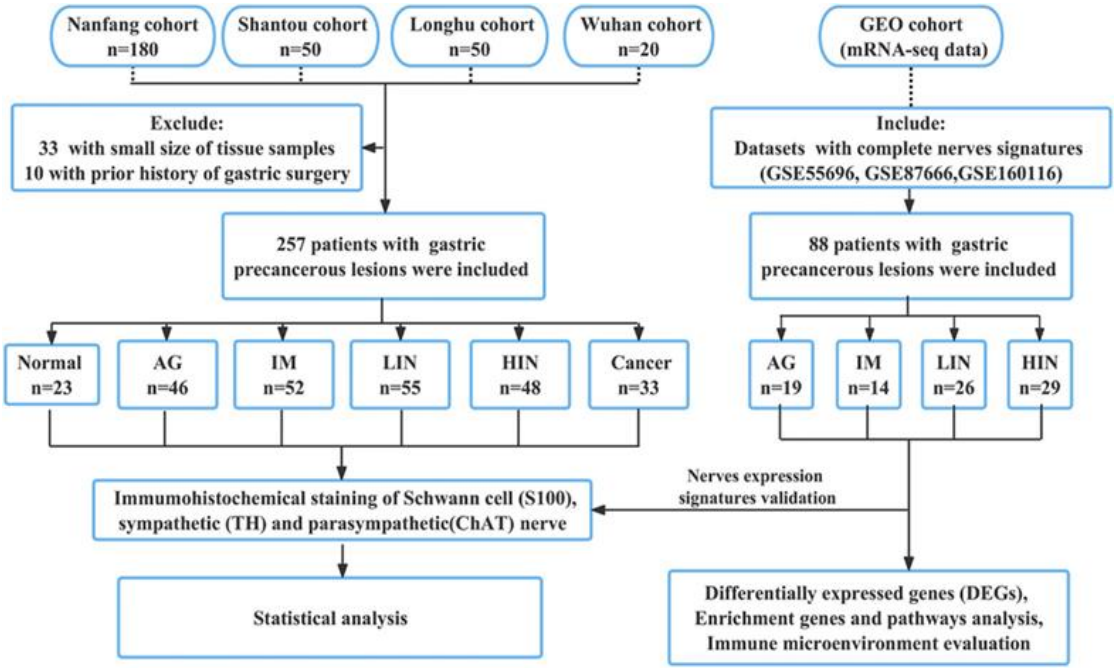

Figure 1. Overview of the research workflow.

Immunohistochemistry and digital measurement of nerve densities

Immunohistochemistry (IHC) served to detect proteins unique to nerves. Markers included S100 for axons, tyrosine hydroxylase (TH) for sympathetic nerves, and ChAT for parasympathetic nerves. A uniform IHC procedure was applied, which included cutting tissue sections, retrieving antigens, blocking nonspecific sites, applying primary and secondary antibodies, and developing the signal with 3,3'-Diaminobenzidine along with hematoxylin counterstain. Digital quantification [17] measured the percentage of immunoreactive area (IRA%) occupied by nerve elements. Whole-slide digital scans were captured with a slide-scanning device under consistent parameters. Two experienced pathologists, unaware of the study groupings, examined all stained slides to classify tissue categories and grade the lesions. Nerve analysis was restricted to the stromal areas associated with the lesions. Fiji ImageJ software processed the staining, applying the Yen algorithm [18] to set optimal thresholds. All laboratory work took place at the Guangdong Provincial Key Laboratory of Precision Medicine for Gastrointestinal Tumor. Full details on reagents and step-by-step procedures appear in the Supplementary Methods.

Evaluation of nerve signatures, pathways, and immune microenvironment

Signatures for the autonomic nervous system (ANS) were confirmed with established marker genes [19]. Differentially expressed genes (DEGs) across GPL subtypes were identified via the "limma" R package, applying criteria of fold change (FC) >1.4 and false discovery rate (FDR) <0.05. Lists of GC driver genes and nerve-cancer interaction genes helped isolate driver-related and nerve-regulated genes showing differential expression. Pathway and functional analyses—including gene ontology (GO) enrichment, gene set enrichment analysis (GSEA), and Gene Set Variation Analysis (GSVA)—were conducted to evaluate tumor-related hallmarks and active routes. The tumor microenvironment (TME) was profiled using single-sample gene set enrichment analysis (ssGSEA) along with curated immune gene sets. Additional information on the bioinformatics approaches and related methods is provided in the Supplementary Methods.

Statistical analysis

All statistical calculations and graphical outputs were generated with IBM-SPSS version 25 and GraphPad Prism version 8. Bioinformatics processing utilized Perl Programming Language (v5.30.0) and R software (4.2.0). The non-parametric Kruskal–Wallis test handled group comparisons. Significant differences in multiple comparisons are denoted by lowercase letters ($p < 0.05$), where groups sharing the same letter show no meaningful difference and groups with different letters are statistically distinct. A p-value threshold of <0.05 defined statistical significance.

Results and Discussion

Baseline patient characteristics and nerve distribution patterns

Every pathological sample was carefully reviewed by pathologists to confirm adequate tissue quantity for immunohistochemistry and digital assessment. As illustrated in **Figure 2a**, specimens obtained from endoscopic biopsies or surgical procedures included at least intact mucosal layers comprising gastric foveola, glands, and muscularis mucosa. Samples lacking sufficient tissue quality were removed from further analysis. Lesion grading followed the updated Sydney system's visual analog scale guidelines [20].

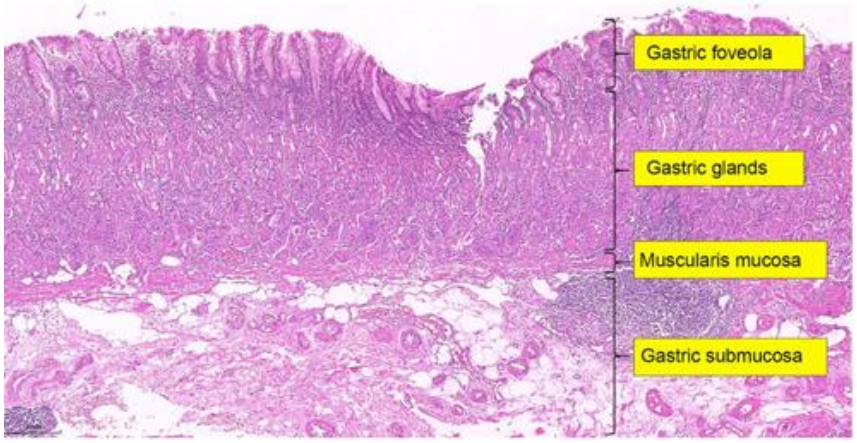

a)

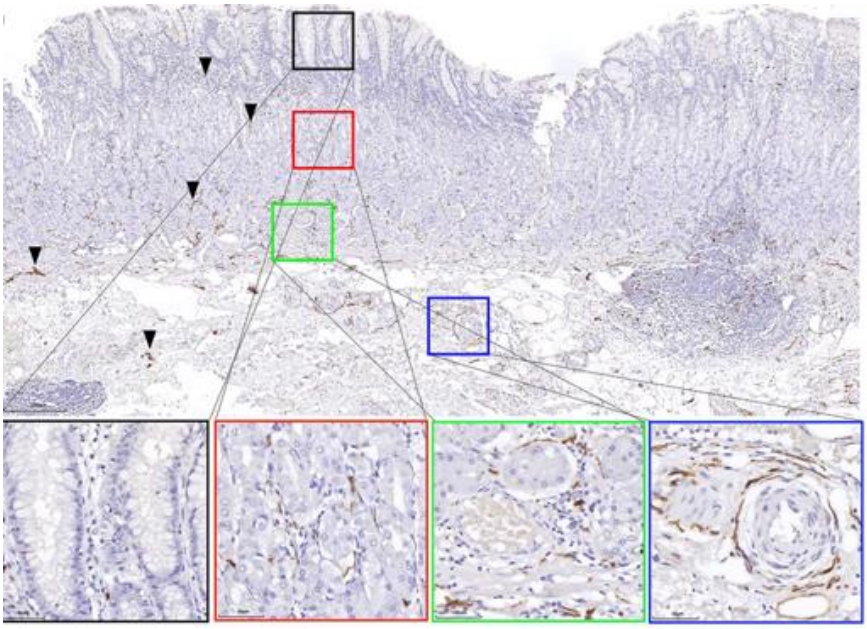

b)

Figure 2. Typical patterns of nerve presence (visualized by S100 staining) across gastric tissue layers. (a) All samples examined in this project included at least a full mucosal layer encompassing the gastric foveola, glandular structures, and muscularis mucosa. (b) Nerve concentrations reached their peak in the muscularis mucosa and submucosal regions, appeared at intermediate levels within the gastric gland layer, and were minimal in the foveolar region. Nerves clustered prominently around arterioles (highlighted by blue square). Scale bar: 250 μm for panel (a) and the top part of (b); 50 μm for the bottom part of panel (b).

The investigation involved 257 individuals with a mean age of 57 years (ranging from 22 to 89 years). Among them, 158 participants (61.5%) were male and 99 (38.5 percent) were female. Most gastric specimens came from the antrum (72.8%), with smaller proportions from the body (11.3 percent) and cardia (7.4 percent). Patient numbers for the AG, IM, LIN, and HIN categories were 46, 52, 55, and 48, respectively. Additionally, 23 samples of normal tissue adjacent to tumors and 33 samples of intestinal-type gastric cancer served as reference controls.

Regarding cohort distribution, 163 patients (63.4%) belonged to the Nanfang group, 42 (16.3%) to the Shantou group, and 42 (16.3%) to the Longhu group.

Staining for nerve elements by IHC showed clear signals in both mucosal and submucosal compartments. In healthy gastric tissue, nerve arrangement displayed a progressive rise moving from the foveolar area through the gland zone and muscularis mucosa into the submucosa, demonstrating a layered increase in density **(Figure 2b)**, (arrows and square). Nerves were especially concentrated near arterioles in the mucosa and submucosa. This same layered pattern of nerve distribution within the stomach wall persisted in tissues showing precancerous changes and in frank tumors.

To evaluate overall nerve abundance, immunohistochemistry targeting S100—a protein expressed by Schwann cells that wrap around most peripheral nerve axons—was conducted on normal, premalignant, and cancerous gastric tissues. Findings indicated low S100 levels in normal samples (0.279, 95 percent confidence interval [CI]: 0.190–0.368), intermediate levels in precancerous samples (1.286, 95 percent CI: 1.122–1.449), and elevated levels in tumor samples (2.727, 95 percent CI: 1.546–3.908). The contrast between normal and precancerous tissues reached high statistical significance ($p < 0.0001$), while the difference between precancerous and tumor tissues approached significance ($p = 0.050$). Staining for ChAT revealed the opposite intensity pattern: weak signals in normal gastric tissue (2.267, 95 percent CI: 1.783–2.752), moderate signals in precancerous tissue (0.729, 95 percent CI: 0.596–0.862), and strong signals in tumor tissue (0.227, 95 percent CI: 0.150–0.305) **(Figure 3)**. In contrast, TH staining followed a declining trend, showing high expression in normal gastric tissue (2.053, 95 percent CI: 1.720–2.386), moderate expression in precancerous tissue (1.804, 95 percent CI: 1.593–2.015), and low expression in tumor tissue (0.166, 95 percent CI: 0.124–0.209). Differences across the three groups were highly significant ($p < 0.0001$).

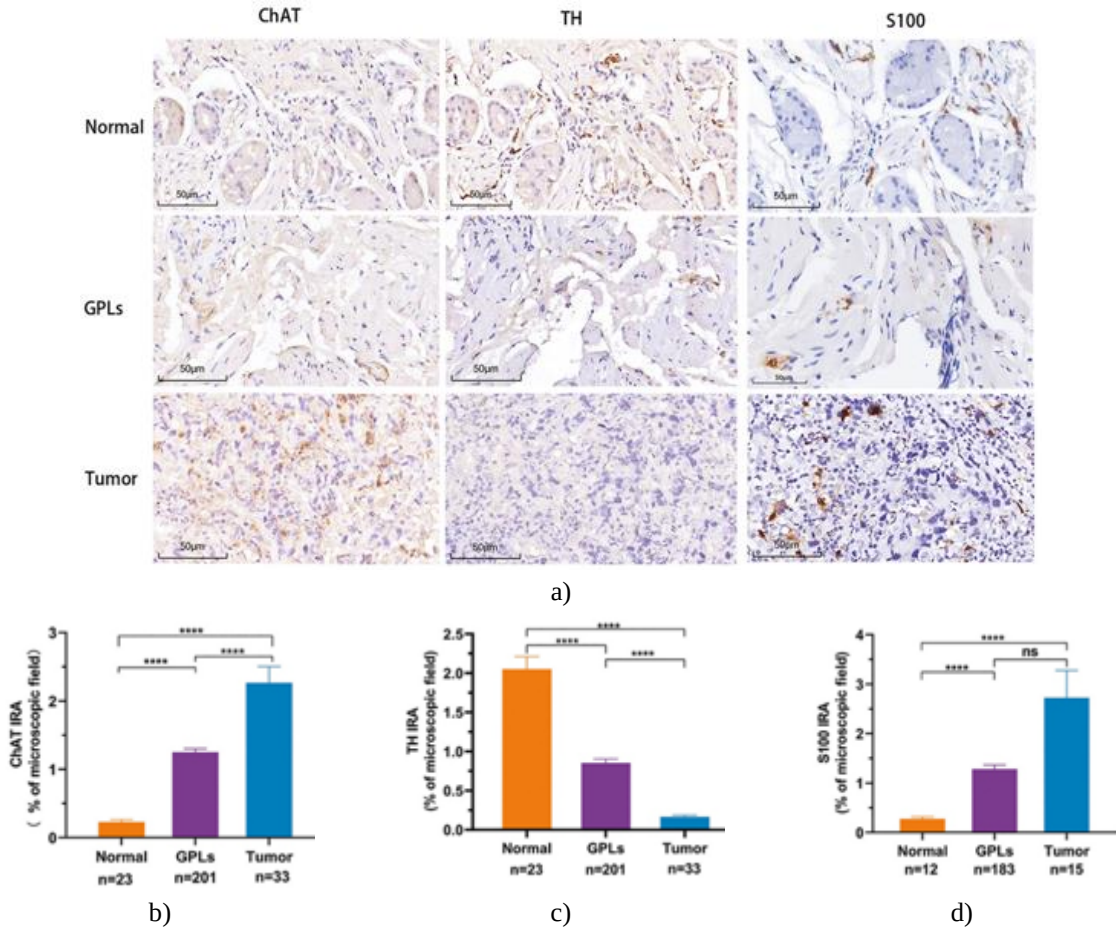

Figure 3. Evaluation of ChAT, TH, and S100 immunoreactivity by immunohistochemistry in healthy gastric mucosa, precancerous conditions, and malignant stomach tissues.

Signals for both ChAT and S-100 appeared weak in normal stomach samples, intermediate in precancerous stages, and reached peak levels in tumor specimens. Application of the Kruskal–Wallis test revealed a highly significant

overall difference in nerve density among the three categories [****p < 0.0001], aside from the S-100 comparison between GPLs and tumor tissues [P = 0.050]. Photomicrographs were taken with a 40× objective lens. Scale bar = 50 μm. [****p < 0.0001]; p value equals 0.05 for GPLs versus tumor. GPLs, gastric precancerous lesions; ns, not significant; TH, tyrosine hydroxylase.

Stratifying analysis of PN, SN and schwann cell

PN displayed substantial variation in its pattern of distribution along the gastric disease continuum **(Figure 4)**. Median IRA% measurements were recorded as 0.180 (95 percent CI: 0.150–0.305) for normal tissue, 0.680 (95 percent CI: 0.596–0.862) for AG, 0.785 (95 percent CI: 0.766–1.010) for IM, 1.260 (95 percent CI: 1.200–1.499) for LIN, 1.935 (95 percent CI: 1.861–2.205) for HIN, and 1.910 (95 percent CI: 1.783–2.752) for tumor. PN density exhibited statistically meaningful distinctions between most subtypes, excluding the pairs AG versus IM [p = 1.00], LIN versus tumor [p = 0.065], and HIN versus tumor [p = 1.000].

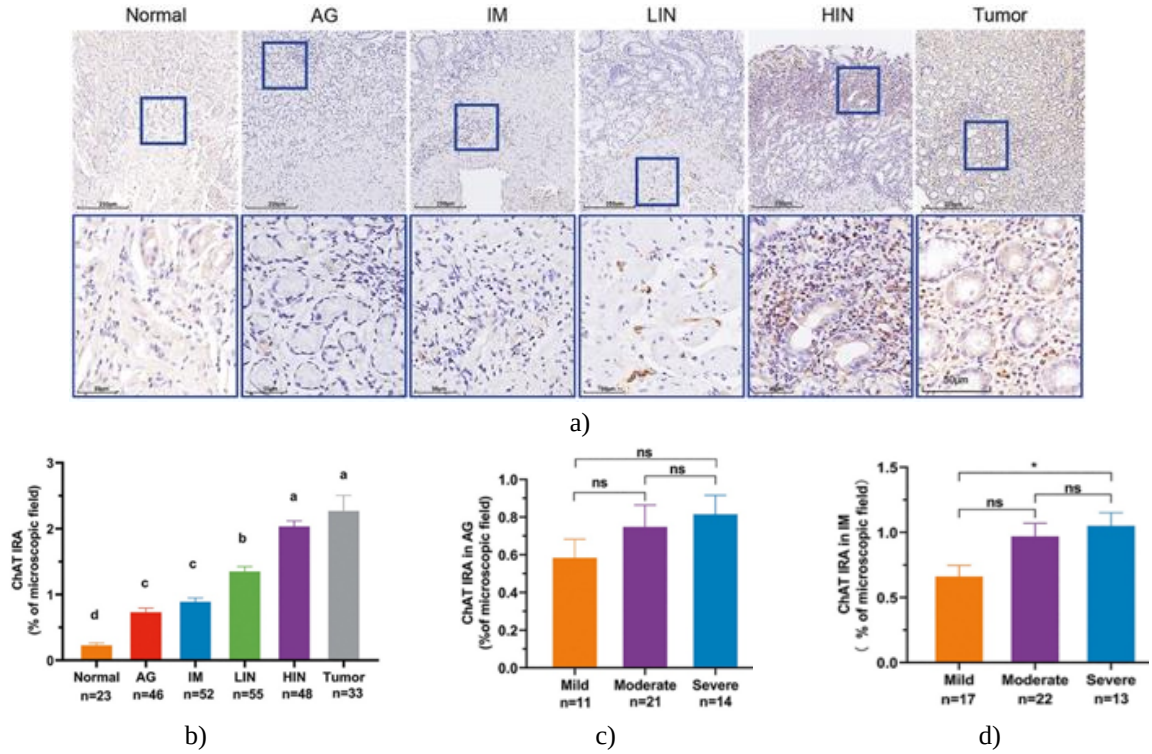

Figure 4. Layered examination of parasympathetic nerve markers throughout normal mucosa, AG, IM, LIN, HIN, and cancerous gastric lesions.

Illustrative immunohistochemical images from the precancerous categories along with comparative statistical evaluation of ChAT immunoreactivity across the spectrum of GPLs. Group differences in nerve density were assessed using the Kruskal–Wallis test. Significance is indicated via letter-based labeling ($p < 0.05$), where distinct letters (a, b, c) signify statistically meaningful differences between categories, while identical letters reflect no significant distinction. AG= atrophic gastritis; GPL= gastric precancerous lesion; HIN= high-grade intraepithelial neoplasia; IM= intestinal metaplasia; LIN= low-grade intraepithelial neoplasia.SN density followed an opposite pattern **(Figure 5)**, progressively declining along the gastric disease continuum. It registered high levels in normal tissue (1.890, 95 percent CI: 1.720–2.386), moderate levels in precancerous stages (AG: 1.780, 95 percent CI: 1.592–2.015; IM: 0.810, 95 percent CI: 0.773–1.037; LIN: 0.550, 95 percent CI: 0.535–0.647; HIN: 0.180, 95 percent CI: 0.163–0.223), and minimal levels in adenocarcinomas (0.130, 95 percent CI: 0.124–0.209). Marked differences in SN density appeared across nearly all subtypes, with the exceptions of normal versus AG [p = 1.00], IM versus LIN [p = 0.394], and HIN versus tumor [p = 1.00].

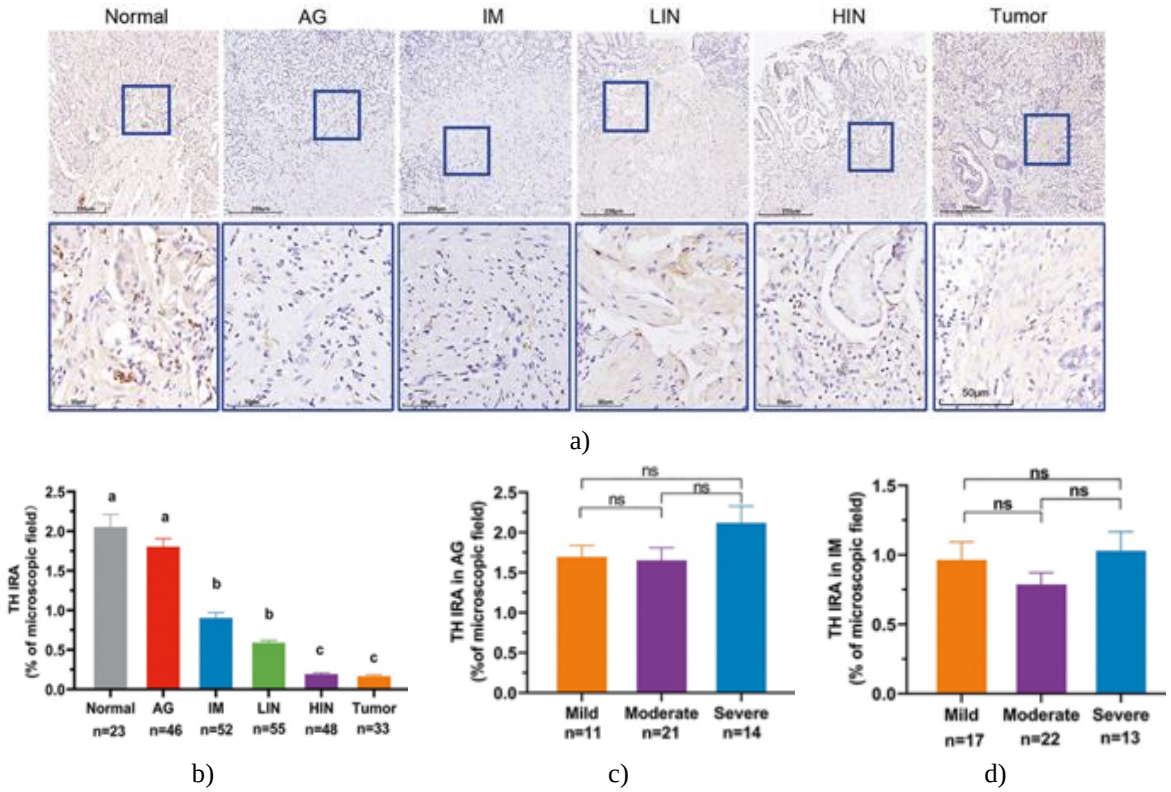

Figure 5. Layered evaluation of sympathetic nerve activity in normal mucosa, AG, IM, LIN, HIN, and tumor tissues.

The panel presents typical immunohistochemical staining images for the precancerous categories together with statistical comparisons of TH staining intensities across the GPL spectrum. Differences in nerve densities were analyzed using the Kruskal–Wallis test. Significant differences ($p < 0.05$) are shown by letter notation, where distinct letters (a, b, c) indicate statistically meaningful differences between groups, while identical letters denote no significant difference. [AG= atrophic gastritis; GPL= gastric precancerous lesion; HIN= high-grade intraepithelial neoplasia; IM= intestinal metaplasia; LIN= low-grade intraepithelial neoplasia; TH= tyrosine hydroxylase.]

S100 staining displays a distribution trend comparable to PN **(Figure 6)**, showing overall increases throughout the GPL spectrum. The median IRA% values for S100 were 0.279 (95 percent CI: 0.190–0.368) in normal tissue, 0.588 (95 percent CI: 0.441–0.734) in AG, 1.201 (95 percent CI: 0.989–1.413) in IM, 1.288 (95 percent CI: 0.919–1.657) in LIN, 2.036 (95 percent CI: 1.629–2.443) in HIN, and 2.727 (95 percent CI: 1.546–3.908) in adenocarcinomas. Nerve densities stayed relatively steady up until the LIN stage, followed by a sharp rise from LIN to HIN that persisted at high levels from HIN into cancer.

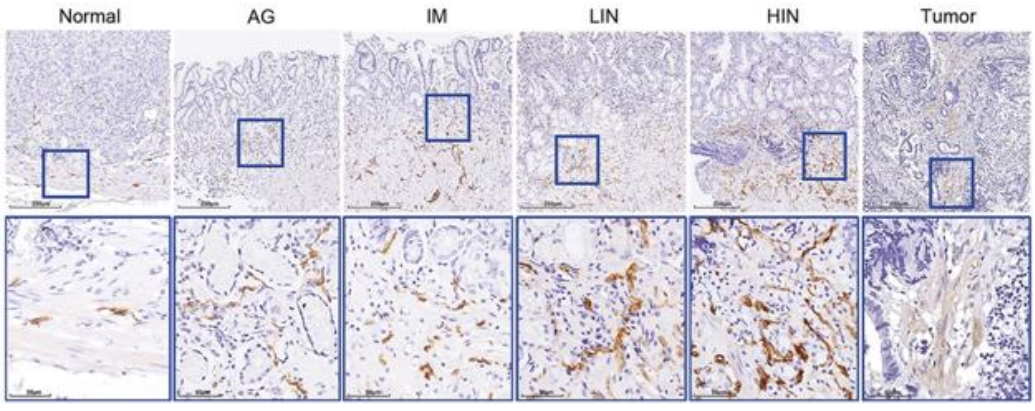

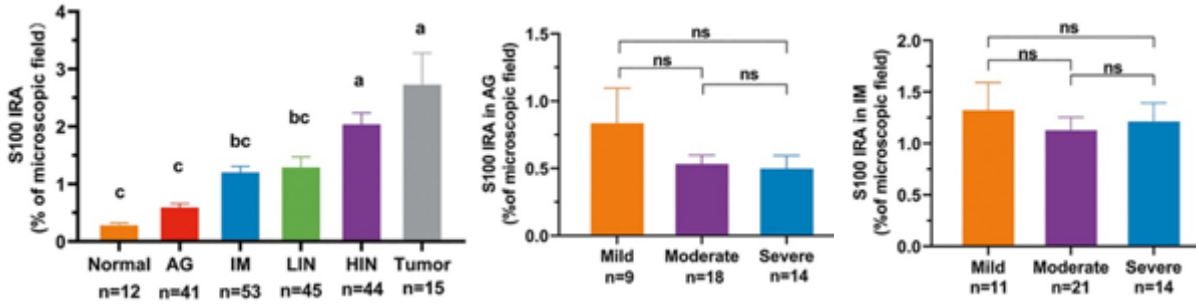

b) c) d)

Figure 6. Tiered assessment of Schwann cell markers in normal tissue, AG, IM, LIN, HIN, and tumor samples.

The figure displays representative immunohistochemical staining images from precancerous categories along with statistical evaluations of S100 staining across the GPL spectrum. Nerve density differences were evaluated via the Kruskal–Wallis test. Significant differences ($p < 0.05$) are marked using letter notation, where different letters (a, b, c) indicate statistically meaningful distinctions between groups, and the same letter signifies no significant difference. [AG= atrophic gastritis; GPL= gastric precancerous lesion; HIN= high-grade intraepithelial neoplasia; IM= intestinal metaplasia; LIN= low-grade intraepithelial neoplasia; TH= tyrosine hydroxylase.]

Subgroup analysis within AG and IM categories showed no notable differences in PN, SN, or S100 densities among mild, moderate, and severe lesions, with the sole exception being ChAT staining between mild and severe IM ($p = 0.022$). The ChAT-TH ratio, which reflects the balance between PN and SN, changes across GPLs. This ratio exhibited no meaningful variation among normal, AG, IM, and LIN stages. However, it rose sharply at the LIN stage and stayed elevated into the tumor stage **(Figure 7a)**. The ChAT-TH ratio demonstrated strong diagnostic performance for distinguishing HIN from LIN (AUC = 0.986) as well as from other precancerous lesions (excluding tumors) **(Figure 7b)**. These results imply that shifts in the ChAT-TH ratio could reflect the degree of precancerous progression and act as a marker for malignant potential.

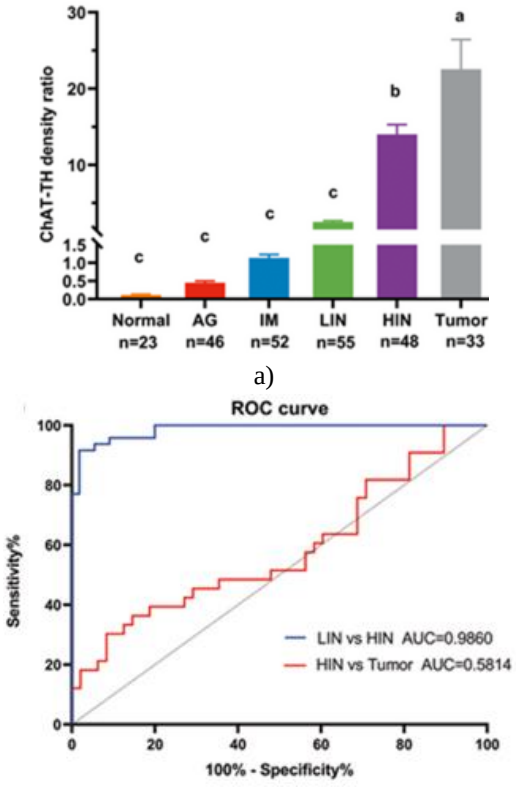

a)

b)

Figure 7. Changes in the ChAT-TH ratio throughout the gastric lesion progression.

(a) Group-wise comparisons of ChAT-TH ratios. (b) Ability of the ChAT-TH ratio to differentiate LIN from HIN, as well as HIN from tumor cases. Group differences were tested with the Kruskal–Wallis method. Significant variations at $p < 0.05$ are shown through letter coding, with distinct letters (a, b, c) marking meaningful separations between categories and matching letters indicating a lack of statistical distinction. [ChAT= choline acetyltransferase; HIN= high-grade intraepithelial neoplasia; IRA= immunoreactive area; LIN= low-grade intraepithelial neoplasia; ns= not significant; TH= tyrosine hydroxylase.]3.3 Validation of autonomic nervous system signatures

Transcriptomic profiling via RNA-seq was carried out on samples spanning four GPL categories (19 AG cases, 14 IM cases, 26 LIN cases, and 29 HIN cases) sourced from GEO datasets. Expression patterns of intratumoral nerve growth (ITNG), sympathetic nervous system (SNS), and parasympathetic nervous system (PNS) signatures were assessed in these GPL subtypes (**Figure 8)**. ITNG and PNS signatures were markedly upregulated from AG onward to HIN ($p < 0.05$), pointing to rising activity of these components moving beyond AG lesions, though no clear distinctions appeared between the IM, LIN, and HIN stages. On the other hand, SNS signature levels dropped substantially from AG to HIN ($p < 0.05$). This pattern matches the IHC-based observations on nerve-specific markers, underscoring the shifting balance of sympathetic and parasympathetic features along the GPL continuum.

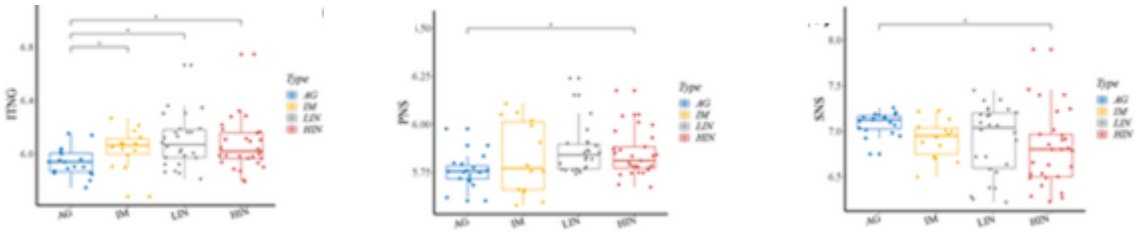

Figure 8. Verification of transcriptional profiles for nerve-related signatures in the gastric precancerous continuum.

The overall ITNG signature (a) and PNS signature (b) rose substantially from AG onward to HIN, in contrast to the SNS signature (c), which declined progressively across this range. [AG= atrophic gastritis; HIN= high-grade intraepithelial neoplasia; ITNG= intratumoral nerve growth; PNS= parasympathetic nervous system; SNS= sympathetic nervous system.]

Identification of DEGs and key nerve-cancer related genes

A collection of 700 DEGs emerged from the comparison of NILM against LIN samples (438 upregulated and 262 downregulated). An additional set of 297 DEGs was uncovered between LIN and HIN tissues (119 upregulated, 178 downregulated). The most prominent upregulated and downregulated genes in both contrasts are visualized in volcano plots **(Figure 9a)**. Overlap examination through Venn diagrams was used to pinpoint genes common to the DEGs, established GC driver genes, and those involved in nerve-cancer interactions. Results from this evaluation **(Figure 9b)** showed seven nerve-linked genes (NTRK3, NRP1, BCL2, CCND1, VEGFA, PLXNA2, and ADRB2) shared within the NILM-to-LIN DEGs. Between LIN and HIN, only two such nerve-linked genes (NTRK3 and MYBL2) overlapped. Moreover, 69 genes **(Figure 9c)** were identified as common DEGs when comparing the LIN-HIN pair with the NILM-HIN pair, implying that LIN already contains genetic features typical of premalignant advancement. When intersecting all three categories (DEGs, GC drivers, and nerve-cancer crosstalk genes), NTRK3 was the only standout core gene. Expression distributions for eight nerve-associated genes appear in half-violin format **(Figure 9d)**. Levels of MYBL2, NRP1, and BCL2 climbed steadily from NILM to LIN and onward to HIN, while CCND1, VEGFA, PLXNA2, and ADRB2 demonstrated declining patterns. NTRK3 followed a unique trajectory, rising initially from NILM to LIN before undergoing a marked reduction in the transition to HIN.

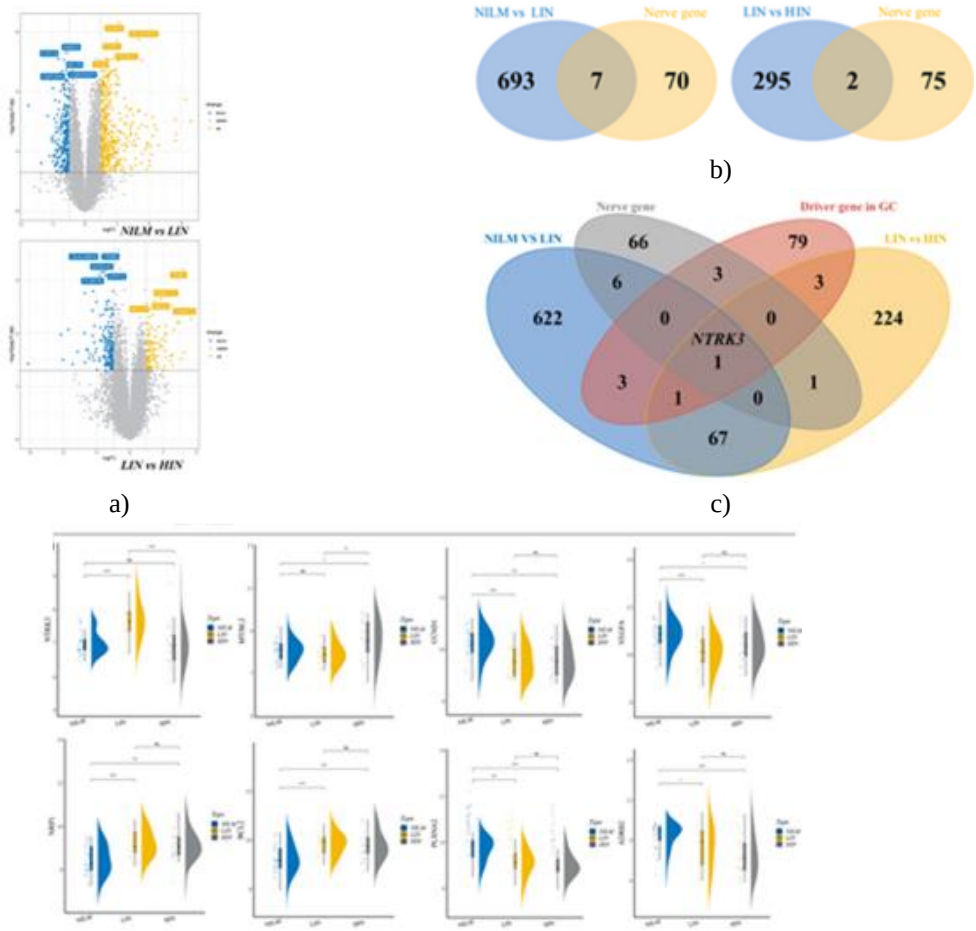

Figure 9. Overview of differentially expressed genes (DEGs) during gastric precancerous progression. (a) Volcano plots highlighting DEGs and the five most prominently upregulated and downregulated genes in contrasts across NILM, LIN, and HIN categories. (b, c) Venn diagrams depicting the intersection of DEGs with GC driver genes and nerve-cancer crosstalk-related genes. (d) Half-violin plots summarizing the expression levels of eight central nerve-associated genes. [GC= gastric cancer; HIN= high-grade intraepithelial neoplasia; LIN= low-grade intraepithelial neoplasia; NILM= negative for intraepithelial lesion or malignancy.]

Biological pathways analysis of GPLs subtypes

Functional annotation through GO analysis demonstrated that the identified DEGs were predominantly linked to granulocyte chemotaxis and migration, neutrophil chemotaxis connected to neutrophil-mediated immunity, along with multiple digestive tract processes **(Figure 10a)**. Further examination via GSEA on Hallmark collections **(Figures 10b and 10c)** and KEGG databases **(Figures 10d and 10e)** revealed that genes upregulated when moving from NILM to LIN were strongly associated with complement-coagulation cascades, broad inflammatory responses, RAS/KRAS signaling, and neuroactive ligand-receptor interactions. Conversely, genes downregulated in this transition showed enrichment in interferon-alpha responses, Notch pathway activity, and DNA replication mechanisms. For the progression from LIN to HIN, upregulated genes were enriched in Myc, VEGF, mTORC1, PI3K/AKT/mTOR, pancreatic cancer, and epithelial signaling pathways triggered by Helicobacter pylori infection. Downregulated genes in this step were enriched in neuroactive ligand-receptor interactions, fatty acid metabolic processes, and Hedgehog signaling. Collectively, the DEG profiles from both transitions converge on shared themes involving inflammatory and immune modulation, neural control mechanisms, and key cancer-promoting signals such as Ras/Kras and PI3K/AKT/mTOR cascades.

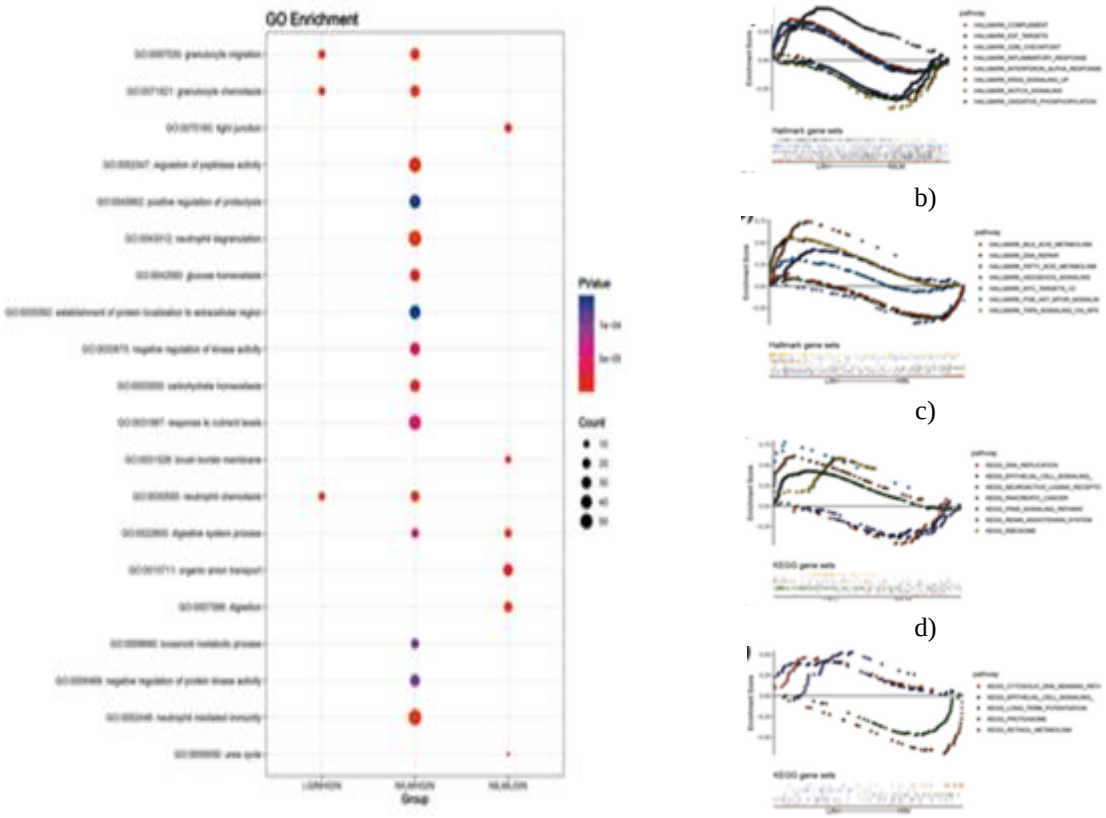

Figure 10. Enrichment analysis of biological pathways.
(a) Gene ontology (GO) results focused on biological processes across GPL subtypes. Gene set enrichment analysis (GSEA) of DEGs using Hallmark gene sets for (b) NILM versus LIN and (c) LIN versus HIN, along with KEGG gene sets for (d) NILM versus LIN and (E) LIN versus HIN. [DEGs= differentially expressed genes; GPLs= gastric precancerous lesions; HIN= high-grade intraepithelial neoplasia; KEGG= Kyoto Encyclopedia of Genes and Genomes; LIN= low-grade intraepithelial neoplasia; NILM= negative for intraepithelial lesion or malignancy.]

GSVA further validated key biological pathways participating in GPL advancement. Pathways tied to inflammation and immune activity—including inflammatory response, complement-coagulation cascades, interferon signaling, and oxidative phosphorylation—were markedly upregulated. In addition, well-established GC-associated routes such as epithelial-to-mesenchymal transition (EMT), Ras/Kras, and mTOR signaling were activated throughout the GPL spectrum. These results reinforce the presence of inflammatory processes accompanied by diverse immune reactions during GPL development. Prominent activated pathways encompass epithelial cell signaling in HP infection, MYC targets, EMT, Ras/Kras, and mTOR. Altogether, the data point to interconnected roles of HP-driven inflammation, neural modulation, and immune signaling during the process of gastric cancer development.3.6 Immune microenvironment exploration

ssGSEA was applied to calculate immune cell infiltration scores and evaluate immune-related markers across different risk categories. Clear variations emerged in the abundance of various immune cell types and biomarkers **(Figure 11a)**. Infiltration levels of aDCs, HLA, and T helper cells displayed an upward trajectory, while CD8+ T cells, natural killer cells, and APC co-inhibition showed notable reductions from NILM through LIN to HIN. This pattern reflects progressive suppression of anti-tumor immune responses as GPLs advance, with the effect being especially pronounced in the transition from NILM to LIN.

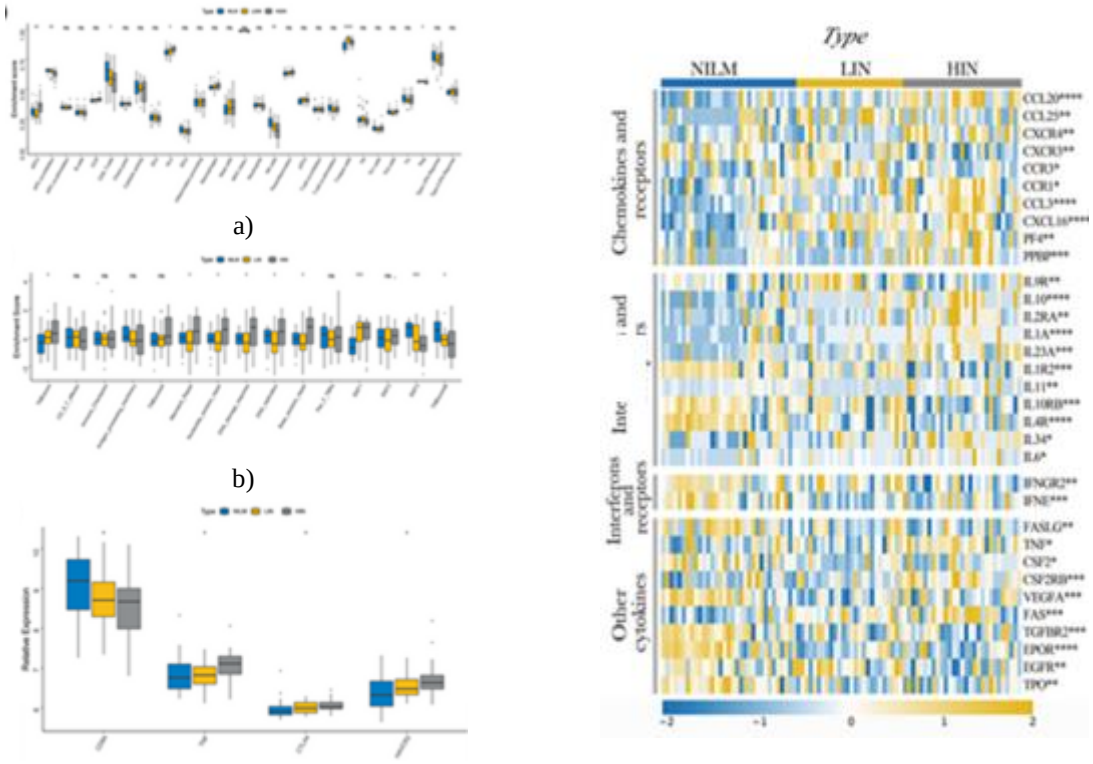

Figure 11. Immune microenvironment assessment.
(a) Box plots derived from single-sample gene set enrichment analysis (ssGSEA) depicting variations in immune cell infiltration levels across NILM, LIN, and HIN categories; (b) gene clusters differentiated according to immune-related signatures, TME scores, and associated biological pathways; (c) variations in the expression of genes linked to immune activation and immune checkpoints across GPL subtypes; (d) heatmap displaying differential expression patterns of chemokines, interleukins, interferons, and their receptors among GPL subtypes. GPLs: gastric precancerous lesions; HIN: high-grade intraepithelial neoplasia; LIN: low-grade intraepithelial neoplasia; NILM: negative for intraepithelial lesion or malignancy.

ssGSEA on gene sets tied to distinct biological functions indicated substantial involvement of stromal-activation signatures, DNA damage and repair signatures, as well as immune activation signatures **(Figure 11b)**.
EMT, a key mechanism in which epithelial cells gain mesenchymal traits associated with invasiveness [21], exhibited markedly elevated levels in LIN and HIN relative to NILM ($p < 0.001$). This points to a progressive shift toward mesenchymal features as lesions advance. EMT pathway activation can suppress the priming of effector T cells and impair their cytotoxic activity [22], which may account for the reduced CD8+ T cell presence observed in the HIN group. Analysis of immune activation and checkpoint gene expression across GPL subtypes revealed that tumor necrosis factor (TNF), a marker of immune activation, rises steadily from NILM through LIN to HIN. Meanwhile, immune checkpoint markers such as CTLA-4 and HAVCR2 also increase progressively **(Figure 11c)**. Elevated levels of these checkpoint molecules facilitate immune evasion in this subtype. These observations are consistent with the biological process and pathway enrichments identified via ssGSEA, reflecting a growing suppression of anti-tumor immune responses during GPL progression.
Immunomodulator expression, encompassing chemokines, interleukins, interferons, and their receptors, was evaluated in the immune microenvironments of GPLs **(Figure 11d)**. LIN and HIN displayed upregulated expression of several chemokines (CCL20, CCL25, CCR1, CCR3, CCL3, CXCL16, and PF4) and interleukins/cytokines (IL10, IL2RA, IL1A, IL23A, IL34, TNF, CSF2RB, and FAS) compared with NILM. In contrast, other interleukins, cytokines, and interferons (IL1R2, IL10RB, IL4R, IFNGR2, IFNE, VEGFA, TGFBR2, EPOR, EGFR, and TPO) were significantly downregulated in the LIN and HIN groups.
Nerves were historically regarded as having minimal influence on tumor development, resulting in their oversight in studies of the tumor microenvironment (TME). However, the identification of novel nerve-related biomarkers and improved research techniques have sparked growing interest in the regulatory functions of nerves in oncology

[23]. Although the significance of nerves in cancer is increasingly acknowledged, their specific contributions in gastric cancer (GC) are only recently being explored [24].

The autonomic nervous system (ANS) comprises sympathetic and parasympathetic divisions that jointly control various physiological activities. Sympathetic nerves trigger the "fight or flight" response, which decreases gastric blood flow and digestive processes. Parasympathetic nerves (PN), conversely, support the "rest and digest" state by promoting digestive activity. These antagonistic functions of sympathetic nerves (SN) and PN extend to the TME [6, 25, 26]. Adrenergic signals promote pathways that drive tumor proliferation, invasion, and spread, whereas cholinergic signals inhibit tumor formation and cancer stem cell properties via the MAPK/EGFR and PI3K/AKT cascades [12, 27].

Recent investigations have highlighted the important contributions of nerves to the initiation and advancement of GC. In a murine GC model, Hayakawa *et al*. [28] showed that gastrointestinal nerves control tumor stem cells through acetylcholine secretion. Acetylcholine from Dclk1+ tuft cells and nerves further induces nerve growth factor (NGF) production in gastric epithelial cells, which promotes neuronal expansion and triggers tumorigenesis via Wnt pathway activation. Blocking downstream NGF/Trk receptor signals and muscarinic receptor-3 can suppress epithelial proliferation and tumor development.

Overall, the tumor-promoting effects of parasympathetic/acetylcholinergic nerves in GC are becoming well-established through both animal models and clinical data from patients after vagotomy [29-31]. In contrast, the role of sympathetic/adrenergic nerves in GC remains debated. Miyato *et al*. [32] analyzed surgically removed GC samples and reported a notable reduction in SN fibers within tumor tissue. This SN loss correlated with poorer clinical features, such as greater invasion depth, increased lymph node involvement, and reduced survival. Comparable results were summarized in a recent review [33]. However, Tatsuta *et al*. [34] demonstrated that chemical sympathectomy with 6-hydroxydopamine, which eliminates catecholaminergic neurons, markedly decreased gastric tumor formation in rats. Additionally, another study linked high SN density to increased tumor recurrence risk [35]. Due to inconsistent results and limited sample sizes, no firm consensus exists on sympathetic signaling in gastric tumor development. The current findings help fill this knowledge gap by detailing shifts in nerve density and distribution throughout GPL stages.

The Correa cascade provides a well-accepted model of gastric carcinogenesis [36]. Examining alterations in nerve types and density within this sequence can clarify nerves' involvement in GC. Earlier research noted dense PN fibers linked to tumor promotion and produced mixed results on SN fiber density in established GC, but no prior studies had directly compared SN and PN or assessed their status in human gastric precancerous conditions. Using immunohistochemistry on matched samples with specific SN and PN markers, this study demonstrates a progressive decline in SN density across precancerous stages, with only sparse SN fibers persisting in GC. PN density, however, rose approximately ninefold in GC compared to normal mucosa. Schwann cell density also increased alongside PN fibers, underscoring their supportive role in neural expansion. Notably, PN and axon densities stayed low through most precancerous phases before sharply rising in late precancerous and early cancerous stages. This pattern likely reflects a modified neo-organogenesis process that incorporates angiogenesis for nutrient delivery and neurogenesis for signaling and coordination during tumor expansion [37].

We introduce the PN-SN ratio as a novel index of disease progression, given the divergent trends of SN and PN in precancerous lesions. This ratio integrates changes in both nerve types: a lower ratio corresponds to reduced risk of progression to cancer, whereas a higher ratio signals greater likelihood of advancement. The PN-SN ratio may thus serve as a useful prognostic tool for assessing precancerous lesion severity and guiding clinical management of GPLs.

In genetically modified mouse models, Zhao *et al*. [30] illustrated that parasympathetic denervation inhibits gastric tumor formation. Miyato *et al*. [32], studying human GC tissues, linked low SN density to increased invasion, lymph node metastasis, and worse survival. Integrating these prior observations with the present results suggests that nerve distribution imbalance arising from remodeling processes may either drive or mark the neoplastic shift in gastric tissue. Faulkner *et al*. [6] characterized the opposing yet linked actions of SN and PN as a Yin-yang form of neural control in cancer. Given the dynamic SN-PN interplay identified here, a similar Yin-yang regulatory pattern is likely operative in GC development.

Bioinformatic examination of GPL transcriptomic profiles uncovered several central nerve-regulatory genes: NTRK3, MYBL2, NRP1, BCL2, CCND1, VEGFA, PLXNA2, and ADRB2. MYBL2 acts as an oncogene in GC, enhancing cell proliferation, blocking apoptosis, and driving tumorigenesis and metastasis through the Wnt/β-catenin pathway [38]. NRP1 functions oncogenically by influencing axon guidance and nervous system development, while also advancing tumor growth via VEGFR interactions with semaphorins and VEGF family

members [39]. PLXNA2 modulates perineural invasion in prostate cancer [40]; its upregulation limits tumor migration and invasion, whereas downregulation enhances these capabilities in melanoma [41]. ADRB2 similarly appears protective, influencing immune regulation in breast cancer [42].

These hub genes likely affect distinct nerve populations through intricate nerve-cancer interactions, resulting in the observed shifts in nerve distribution. Notably, MYBL2, NRP1, and BCL2 expression gradually increased across GPLs, implicating them in carcinogenesis. PLXNA2 and ADRB2, however, showed declining trends, consistent with potential tumor-suppressive roles. This indicates that nerves interact with diverse molecular cues to exert varied effects, with gene expression changes possibly orchestrating the neurodynamic alterations.

GSEA and GSVA analyses highlighted strong activation of inflammatory and immune pathways, epithelial-to-mesenchymal transition, and epithelial cell signaling in the Helicobacter pylori infection pathway. Established GC-associated routes, including VEGF, Ras/Kras, mTOR, and Wnt signaling, were also enriched across GPL stages. A literature survey reinforced the relevance of MAPK/ERK, PI3K/AKT/mTOR, and Wnt cascades as key nerve-modulating pathways in GPL advancement and nerve-precancer interactions.

Among the identified genes, neurotrophic receptor tyrosine kinase 3 (NTRK3, also known as TrkC) stood out. NTRK3 is part of the neurotrophin receptor family (NTRK1–3) and is essential for central nervous system development during embryogenesis [43]. It binds NT-3 and activates downstream cascades such as mTOR and Wnt/β-catenin, which govern cell differentiation, growth, and survival in GC [44-46]. NTRK3 can act as either an oncogene or tumor suppressor. While NTRK3 fusions drive oncogenesis in multiple solid tumors [47], it can also suppress tumors; for example, epigenetic silencing of NTRK3 is common in colorectal cancer, and restoring its expression promotes apoptosis in these cells [48]. Neurotrophin binding to TRK receptors leads to dimerization, phosphorylation, and activation of PI3K/AKT/mTOR, RAS/RAF/MAPK/ERK, and Wnt pathways [43-45]. Pathway enrichment in GPL subtypes underscores NTRK3's important contribution to disease progression.

In summary, pathway findings support the idea that GPL initiation stems from inflammation-driven gastric mucosal injury, especially in Helicobacter pylori-associated gastritis. This triggers immune responses and nerve system engagement. Nerves participate actively in pathways such as ERK, mTOR, and Wnt, thereby shaping the TME. These multifaceted neurobiological events ultimately drive precancerous progression. Nevertheless, because these conclusions derive exclusively from bioinformatics, additional experimental validation and mechanistic investigations are necessary.

This investigation has several constraints. The primary limitation is its reliance on quantitative immunohistochemistry combined with bioinformatics validation. The bioinformatics component offers only an initial exploration of candidate genes and pathways potentially involved in nerve regulation, without a comprehensive mechanistic explanation of the molecular processes driving shifts in nerve density throughout GPL progression. Furthermore, the relatively modest sample size raises the possibility of selection bias affecting the outcomes. Lastly, because all specimens were obtained retrospectively, collection protocols were not standardized, leading to inconsistencies in tissue size and section thickness. Given that nerves are predominantly located in the muscularis mucosa and submucosa, such variations could introduce inconsistencies in the quantification of nerve densities via immunostaining.

This work advances knowledge regarding the involvement of nerves in gastric precancerous lesions and supports the discovery of new treatment targets. Modulating the nervous system and its interplay with malignant cells represents an encouraging direction in oncology. The study yields three main theoretical contributions. First, given the high prevalence of Helicobacter pylori infection and associated precancerous changes, patterns of nerve distribution could help classify patients and identify those at elevated risk, enabling earlier intervention. Second, the combined influence of parasympathetic and sympathetic nerves in gastric cancer may provide a more robust marker for assessing tumor behavior and patient prognosis. Third, in light of the current scarcity of effective therapies for GPLs, interventions directed at specific neural pathways could represent an innovative strategy for managing precancerous conditions and averting progression to gastric cancer.

Continued research into the relationship between nerves and GPLs is essential for developing new treatments and enhancing patient prognosis. A key priority is to clarify the precise molecular mechanisms responsible for the observed fluctuations in nerve density during GPL advancement. Techniques such as single-cell RNA sequencing could uncover heterogeneity within nerve populations and define their contributions to disease evolution. Further exploration of signaling interactions between nerves and cancer cells, with emphasis on core nerve-associated genes including NTRK3, MYBL2, and NRP1, will be important. In addition, large-scale prospective clinical studies with thoroughly documented patient groups are required to confirm the utility of sympathetic and

parasympathetic nerve assessments, along with the PN-SN ratio, for tailoring individualized management strategies in individuals with GPLs and gastric cancer. Research into innovative therapies that target the nervous system and interrupt nerve-cancer communication also shows strong potential for halting gastric cancer development and improving survival rates. Pursuing these lines of inquiry should provide deeper insight into neurobiological aspects of gastric tumor formation and pave the way for groundbreaking therapeutic approaches.

Conclusion

In summary, the present study broadens insight into the density and spatial arrangement of sympathetic and parasympathetic nerves across various phases of gastric precancerous lesions. We documented a steady reduction in sympathetic nerve density alongside a rise in parasympathetic nerve density, progressing from normal mucosa through precancerous stages to invasive cancer. The reciprocal changes between these two nerve types point to a Yin-yang style of neural control in gastric cancer. Several critical nerve-regulatory genes were pinpointed, along with their participation in the MAPK/ERK, PI3K/AKT/mTOR, and Wnt signaling cascades during GPL evolution. These results emphasize the value of understanding nerve-tumor cell interactions for better prevention and management of gastric cancer. They also open doors for future clinical applications centered on nervous system modulation and interference with nerve-cancer signaling.

Acknowledgments: None

Conflict of Interest: None

Financial Support: None

Ethics Statement: None

References

1. Correa P. Human gastric carcinogenesis: a multistep and multifactorial process—First American Cancer Society Award Lecture on Cancer Epidemiology and Prevention. Cancer Res. 1992;52(24):6735-40.
2. Oya Y, Hayakawa Y, Koike K. Tumor microenvironment in gastric cancers. Cancer Sci. 2020;111(8):2696-707.
3. Quail DF, Joyce JA. Microenvironmental regulation of tumor progression and metastasis. Nat Med. 2013;19(11):1423-37.
4. Hirata E, Sahai E. Tumor microenvironment and differential responses to therapy. Cold Spring Harb Perspect Med. 2017;7(7):a026781.
5. Baghban R, Roshangar L, Jahanban-Esfahlan R, Seidi K, Ebrahimi-Kalan A, Jaymand M, et al. Tumor microenvironment complexity and therapeutic implications at a glance. Cell Commun Signal. 2020;18(1):59.
6. Faulkner S, Jobling P, March B, Jiang CC, Hondermarck H. Tumor neurobiology and the war of nerves in cancer. Cancer Discov. 2019;9(6):702-10.
7. Monje M, Borniger JC, D'Silva NJ, Deneen B, Dirks PB, Fattahi F, et al. Roadmap for the emerging field of cancer neuroscience. Cell. 2020;181(2):219-22.
8. Venkataramani V, Tanev DI, Strahle C, Studier-Fischer A, Fankhauser L, Kessler T, et al. Glutamatergic synaptic input to glioma cells drives brain tumour progression. Nature. 2019;573(7775):532-8.
9. Zeng Q, Michael IP, Zhang P, Saghafinia S, Knott G, Jiao W, et al. Synaptic proximity enables NMDAR signalling to promote brain metastasis. Nature. 2019;573(7775):526-31.
10. Mauffrey P, Tchitchek N, Barroca V, Bemelmans AP, Firlej V, Allory Y, et al. Progenitors from the central nervous system drive neurogenesis in cancer. Nature. 2019;569(7758):672-8.
11. Amit M, Takahashi H, Dragomir MP, Lindemann A, Gleber-Netto FO, Pickering CR, et al. Loss of p53 drives neuron reprogramming in head and neck cancer. Nature. 2020;578(7795):449-54.
12. Renz BW, Tanaka T, Sunagawa M, Takahashi R, Jiang Z, Macchini M, et al. Cholinergic signaling via muscarinic receptors directly and indirectly suppresses pancreatic tumorigenesis and cancer stemness. Cancer Discov. 2018;8(11):1458-73.

13. Schledwitz A, Xie G, Raufman JP. Muscarinic receptors and the control of proliferation in the gastrointestinal tract. J Clin Invest. 2021;131(8):e143776.
14. Jiang SH, Zhang S, Wang H, Xue JL, Zhang ZG. Neural regulation of the tumor microenvironment in gastrointestinal cancers. Cancer Lett. 2022;535:215610.
15. Chen YF, Wang SY, Le PH, Chen TH, Kuo CJ, Lin CJ, et al. Clinical significance of nerve density and its correlation with prognosis in pancreatic ductal adenocarcinoma. J Pers Med. 2022;12(6):962.
16. Zhao B, Lv W, Mei D, Luo R, Bao S, Huang B, et al. Perineural invasion in gastric cancer: a systematic review and meta-analysis. J Clin Pathol. 2020;73(9):544-51.
17. Laghi L, Bianchi P, Miranda E, Balladore E, Pacetti V, Grizzi F, et al. CD3+ cells at the invasive margin of colorectal cancer predict prognosis. Lancet Oncol. 2009;10(9):877-84.
18. Yen JC, Chang FJ, Chang S. A new criterion for automatic multilevel thresholding. IEEE Trans Image Process. 1995;4(3):370-8.
19. Zhang JF, Sheng H, Chen J, Mohammadpour H, Ma SJ, Farrugia MK, et al. The role of the sympathetic nervous system in tumor progression and metastasis. Cancers (Basel). 2022;14(10):2541.
20. Dixon MF, Genta RM, Yardley JH, Correa P. Classification and grading of gastritis: the updated Sydney System. Am J Surg Pathol. 1996;20(10):1161-81.
21. Dongre A, Weinberg RA. New insights into the mechanisms of epithelial–mesenchymal transition and implications for cancer. Nat Rev Mol Cell Biol. 2019;20(2):69-84.
22. Tauriello DVF, Palomo-Ponce S, Stork D, Berenguer-Llergo A, Badia-Ramentol J, Iglesias M, et al. TGFβ drives immune evasion in genetically reconstituted colon cancer metastasis. Nature. 2018;554(7693):538-43.
23. Wang H, Zheng Q, Lu Z, Wang L, Ding L, Xia L, et al. The role of the autonomic nervous system in the tumor microenvironment. Cell Death Discov. 2021;7(1):76.
24. Holland AM, Bon-Frauches AC, Keszthelyi D, Melotte V, Boesmans W. The enteric nervous system in gastrointestinal disease. Cell Mol Life Sci. 2021;78(10):4713-33.
25. Silverman DA, Martinez VK, Dougherty PM, Myers JN, Calin GA, Amit M. Cancer neuroscience: state of the field, emerging directions. Cancer Res. 2021;81(6):1431-7.
26. Hutchings C, Phillips JA, Djamgoz MBA. Nerve–cancer interactions: the role of the autonomic nervous system in the tumor microenvironment. Biochim Biophys Acta Rev Cancer. 2020;1874(2):188411.
27. Renz BW, Takahashi R, Tanaka T, Macchini M, Hayakawa Y, Dantes Z, et al. β2-adrenergic-neurotrophin feedforward loop promotes pancreatic cancer. Cancer Cell. 2018;33(1):75-90.
28. Hayakawa Y, Sakitani K, Konishi M, Asfaha S, Niikura R, Tomita H, et al. Nerve growth factor promotes gastric tumorigenesis through aberrant cholinergic signaling. Cancer Cell. 2017;31(1):21-34.
29. Bahmanyar S, Ye W, Dickman PW, Nyrén O. Long-term risk of gastric cancer by subsite after Helicobacter pylori eradication: a population-based cohort study. Am J Gastroenterol. 2007;102(6):1185-91.
30. Zhao CM, Hayakawa Y, Kodama Y, Muthupalani S, Westphalen CB, Andersen GT, et al. Denervation suppresses gastric tumorigenesis. Sci Transl Med. 2014;6(250):250ra115.
31. Wang K, Zhao X, Liu J, Zhang R, Li J. The role of neuroimmune crosstalk in cancer progression. Biochim Biophys Acta Rev Cancer. 2020;1873(2):188313.
32. Miyato H, Kitayama J, Ishigami H, Kaisaki S, Nagawa H. Sympathetic nerve stimulation promotes tumor progression in colon cancer. Ann Surg Oncol. 2011;18(8):2281-8.
33. Kamiya A, Hiyama T, Fujimura A, Yoshikawa S. Autonomic nervous system and cancer: a review. Clin Auton Res. 2021;31(2):165-77.
34. Tatsuta M, Iishi H, Baba M, Taniguchi H. Inhibition of gastric carcinogenesis by chronic denervation of the stomach in rats. Int J Cancer. 1992;51(5):767-70.
35. Schmitd LB, Perez-Pacheco C, D'Silva NJ. The neural microenvironment in oral cancer. FASEB BioAdv. 2021;3(10):773-85.
36. Moss SF. The clinical evidence linking Helicobacter pylori to gastric cancer. Cell Mol Gastroenterol Hepatol. 2016;3(2):183-91.
37. Dlamini Z, Mathabe K, Padayachy L, Marima R, Evangelou G, Syrigos KN, et al. The role of the nervous system in cancer progression. Cancers (Basel). 2021;13(9):2138.
38. Deng Q, Wu L, Li Y, Zou L. The role of nerves in the tumor microenvironment of gastrointestinal cancers. Adv Clin Exp Med. 2021;30(9):957-66.
39. Liu SD, Zhong LP, He J, Zhao YX. Advances in research on the interaction between the nervous system and tumors. Chin Med J (Engl). 2021;134(5):508-15.

40. Yin L, Li J, Wang J, Pu T, Wei J, Li Q, et al. Neurotransmitters and their receptors in the tumor microenvironment: implications for cancer therapy. Oncogene. 2021;40(8):1362-75.
41. Tyumentseva A, Averchuk A, Palkina N, Zinchenko I, Moshev A, Savchenko A, et al. The nervous system and cancer: cross-talk and therapeutic implications. Front Oncol. 2021;11:732501.
42. Wei X, Chen L, Yang A, Lv Z, Xiong M, Shan C. The role of the autonomic nervous system in tumor immunity. Transl Cancer Res. 2021;10(12):5280-94.
43. Arévalo JC, Wu SH. Neurotrophin signaling: many exciting surprises! Cell Mol Life Sci. 2006;63(13):1523-37.
44. Khotskaya YB, Holla VR, Farago AF, Mills Shaw KR, Meric-Bernstam F, Hong DS. Targeting TRK family proteins in cancer. Pharmacol Ther. 2017;173:58-66.
45. Chu YH, Dias-Santagata D, Farahani AA, Boyraz B, Faquin WC, Nosé V, et al. Clinicopathologic and molecular characterization of NTRK-rearranged thyroid carcinoma. Mod Pathol. 2020;33(11):2186-97.
46. Colozza G, Jami-Alahmadi Y, Dsouza A, Tejeda-Muñoz N, Albrecht LV, Sosa EA, et al. Wnt-inducible Lrp6-APEX2 interaction identifies Wnt-regulated proteins. Sci Rep. 2020;10(1):21555.
47. Westphalen CB, Krebs MG, Le Tourneau C, Sokol ES, Maund SL, Wilson TR, et al. Pan-cancer analysis of NTRK fusions identifies novel clinical associations and evidence for frequent co-occurrence. npj Precis Oncol. 2021;5(1):69.
48. Luo Y, Kaz AM, Kanngurn S, Welsch P, Morris SM, Wang J, et al. NTRK3 is a potential tumor suppressor gene commonly inactivated by epigenetic mechanisms in colorectal cancer. PLoS Genet. 2013;9(7):e1003552.